Modeling Mass Transfer with Enzymatic Reaction in Electrochemical Multilayer Microreactors

Saliha Bacha, Marielle Montagné, and Alain Bergel
Laboratoire de Génie Chimique UMR CNRS 5503, Université Paul Sabatier, 31062 Toulouse cedex, France

Electrochemical biosensors were used to develop a numerical model of transient mass transfer coupled with enzymatic reactions in thin multilayer microstructures. A finite volume method integrates the partial derivative mass-balance equations making the model very versatile. With a multilayer physical description, general nonlinear enzymatic kinetics and efficient space discretization, the model could be applied to various devices under a broad range of physicochemical conditions. Theoretical results were validated according to experimental data obtained with three different biosensors involving homogeneous or heterogeneous enzymatic catalyses. Model predictions are further discussed for a bienzymatic immobilized enzyme system. The biosensor transient behavior depended strongly on the location of the enzymes in the device and on the mass-transport features. A transient maximum on the current-time curves was predicted accurately by the model. This could be used to improve the biosensor performance. The model can also be a useful framework for designing new electrochemical microreactors.

Introduction

Microtechnology opens promising new opportunities for chemical and biochemical microsystems at the micrometer or nanometer scale (Ehrfeld et al., 1988). It may be possible that microreactors connected by microfluidic devices (Van de Pol et al., 1990; Gass et al., 1994) could permit a complex synthesis process to be finely controlled, avoiding side reactions and resulting in extraordinarily high selectivity. Microreactors would make it possible to perform many cost-effective trials, consuming minimal amounts of substances, for quick screening (Ehrfeld and Wegner, 1995), which would be particularly useful in biotechnology (Walker et al., 1994).

Amperometric electrochemical sensors are examples of microreactors. Holding the electrode potential at an appropriate value to ensure fast oxidation or reduction of the electroactive species makes it possible to precisely monitor and control the mass flux of this species at the electrode surface. Thin layer electrochemical reactors correspond to the simplest electrochemical microreactor configuration. They consist of a single electrolyte layer generally bordered by the electrode on one side and an inactive wall on the other. They have been widely used to analyze electrochemical kinetics or homogeneous kinetics coupled with electronic transfer (Plichon and Laviron, 1976; Laviron and Roullier, 1985). The membrane-covered rotating electrode, which was designed to study membrane permeability (Gough and Leypoldt, 1979) or immobilized enzyme kinetics (Tse et al., 1987), represents another kind of analytical microreactor. According to the same principle, multilayer enzymatic biosensors consist of one or several membrane(s) and electrolyte layer(s) juxtaposed against the electrode surface with enzymes confined free in solution or immobilized in different parts of the device (Scheller and Schubert, 1992). When the sensor is dipped into the solution to be assayed, the analyte diffuses through the device and is involved in the enzymatic reaction(s). Its flux is thus transformed into the flux of an electroactive species which is detected amperometrically at the electrode surface. Thanks to high enzymatic selectivity, these sensors are able to recognize a very specific substrate in a complex mixture and deliver a current directly proportional to its concentration, with a very short response time because of their restricted dimensions.

For simulating classic electrochemical reactors, it is usually assumed that steady state is reached inside the diffusion film near the electrode surface, where all transfers and kinetics

Correspondence concerning this article should be addressed to Alain Bergel.

are faster than concentration changes in the bulk solution (Bauer et al., 1981; Weise et al., 1986; Labrune and Bergel, 1992). In contrast, transient simulation is essential for microreactors because all parts have dimensions close to those of a diffusion layer. Modeling transient behavior has already been proposed for simple configurations, such as a thin-layer reactor (Devaux et al., 1995) or membrane-covered rotating electrode (Gough and Leypoldt, 1980). A finite volume method, essentially used in heat-transfer simulations (Patankar, 1980; Shih, 1984) has recently been used to model mass transfer in multilayer electrochemical systems (Bacha et al., 1993). The versatility of the discretization method permits the space grid to be freely reduced or enlarged in any part of the systems without limitation. The method is thus particularly efficient in accounting for steep gradients induced by surface reactions as they occur in immobilized enzyme multilayer biosensors. The objective of this work is to adapt this numerical method to bienzymatic electrochemical sensors in order to demonstrate the usefulness of this method for such microsystems, and to give insight to transient behavior of multilayer microreactors. After testing the model on a monoenzymatic sensor, devices involving two different enzymatic catalyses at different sites are analyzed.

Theory

Physical description

The general physical description of a bienzymatic amperometric biosensor is shown in Figure 1, a scheme common to most electrochemical biosensor designs (Buerk, 1993). For immobilized-enzyme sensors, the enzymes are covalently linked to the membrane surface or homogeneously immobilized inside it. The electrolyte layer between the electrode and the membrane is generally unavoidable, because the membrane is only held mechanically against the electrode by a silicone O-ring. In all cases, there is a diffusive layer adjacent to the outer membrane surface. Among the numerous possible combinations, five immobilized enzyme arrangements were investigated (Figure 2):

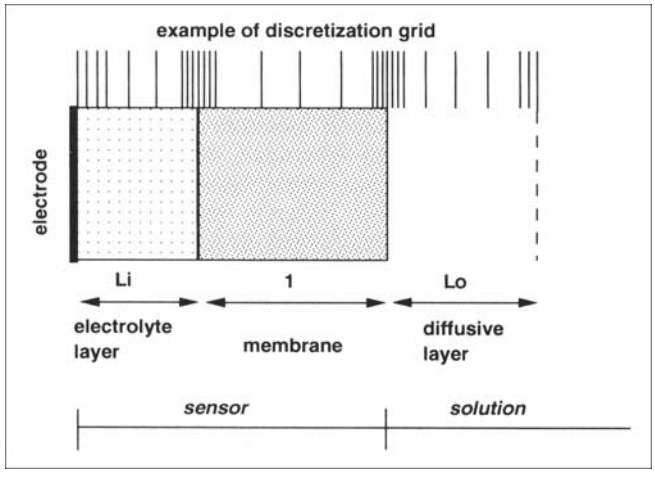

Figure 1. General multilayer scheme for a bienzymatic biosensor.

A finer discretization mesh is chosen near the interfaces where an enzyme could be linked, and at the surface of the electrode.

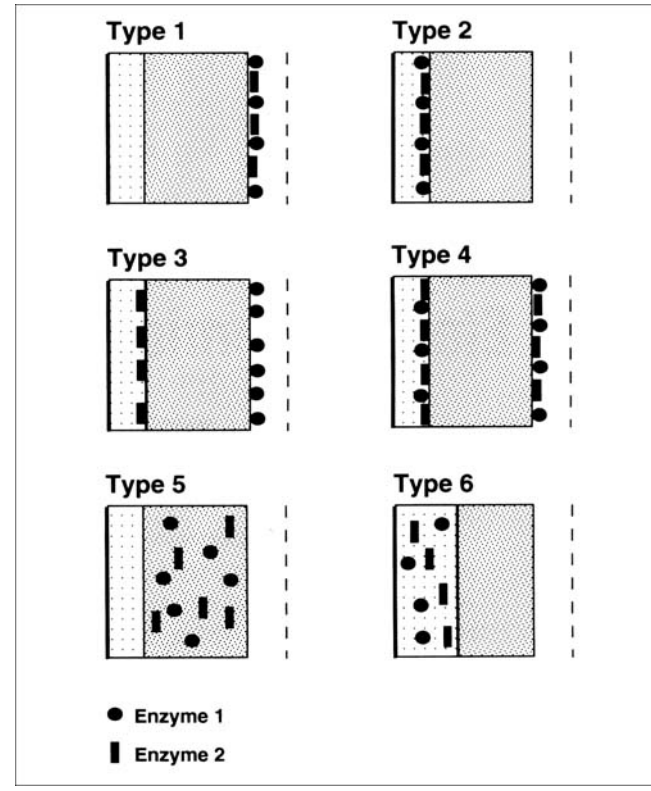

Figure 2. Different bienzymatic biosensor types used in the study.

- Both enzymes linked to the outer membrane surface, i.e., the side turned towards the solution (Type 1)
- Both enzymes linked to the inner membrane surface (Type 2)
- One enzyme linked to the outer membrane surface, the other to the inner surface (Type 3)
- Both enzymes linked to the inner and outer surfaces (Type 4)
- Both enzymes immobilized inside the membrane (Type 5)

In free-enzyme sensors, the enzymes are not immobilized, but confined in an electrolyte layer between the electrode and the membrane (Type 6). All the species except the enzymes are able to diffuse through the membrane. Enzymes either free in solution (Type 6) or immobilized inside the membrane (Type 5) were assumed to be homogeneously distributed.

The electrode was held at a constant potential to oxidize or reduce the electroactive species. Only the oxidation case was studied; however, reduction is quite similar. The whole bienzymatic system consists of two successive enzymatic reactions:

$$S + \gamma_1 \mathrm{Ox}_1 \xrightarrow{E_1} P + \gamma_1 \mathrm{Red}_1$$

$$\mathrm{Red}_1 + \gamma_2 \mathrm{Ox}_2 \xrightarrow{E_2} \mathrm{Ox}_1 + \gamma_2 \mathrm{Red}_2$$

Detection is performed by oxidizing Red_2 at the electrode surface

$$\mathrm{Red}_2 \rightarrow \mathrm{Ox}_2 + e^-$$

When a monoenzymatic system was considered, only the second enzymatic reaction associated with the electrochemical reaction was used, and Red_1 was considered the substrate. The kinetics of the enzymatic reactions were assumed to be of the "ping pong" type, which is a simple kinetic form currently used for two substrate reactions (Dixon and Webb, 1979)

$$\text{rate} = \frac{r_{\max}}{1 + \dfrac{K_S}{[S]} + \dfrac{K_{\mathrm{Ox}}}{[\mathrm{Ox}]}} \tag{1}$$

where $r_{\max}$ is the maximum activity of the enzyme, and K_S and K_{Ox} are the Michaelis constants of the two species involved in the reaction ($\mathrm{mol \cdot m^{-3}}$). The nonlinearity of the kinetics, the steep concentration gradients located at different parts of the sensor and the multilayer structure help to explain the lack of a general transient model.

Transient mass balance equations

The expressions for the two dimensionless groups ϕ^2_{mo} and Da_{mo} were quite close to the square of the Thiele modulus ϕ^2 and the Damköhler number Da, respectively. These numbers express the ratio of the potential reaction rate without mass-transport limitations to the maximum diffusion rate. For the second enzyme, $\phi^2_{2\mathrm{mo}}$ and $Da_{2\mathrm{mo}}$ were the maximum values of ϕ^2 and Da relative to Ox_2

$$\phi_2^2 = \frac{\dfrac{r^{ho}_{2\max}\,\delta_m^2}{D^m_{\mathrm{Ox}2}[\mathrm{Ox}_2]^b}}{1 + K_{\mathrm{Red}1}/[\mathrm{Red}_1]^b + K_{\mathrm{Ox}2}/[\mathrm{Ox}_2]^b} \quad \text{(homogeneous)} \tag{2}$$

$$Da_2 = \frac{\dfrac{r^{he}_{2\max}\,\delta_m}{D^m_{\mathrm{Ox}2}[\mathrm{Ox}_2]^b}}{1 + K_{\mathrm{Red}1}/[\mathrm{Red}_1]^b + K_{\mathrm{Ox}2}/[\mathrm{Ox}_2]^b} \quad \text{(heterogeneous)} \tag{3}$$

The modified parameters ϕ^2_{mo} and Da_{mo} were used for simplicity.

The system is fully described by the transient mass balance equations relative to S, Red_1, Ox_1, Red_2, and Ox_2. The mass-balance equations in a reactive layer and the balance of the mass flux at the membrane/diffusion-layer interface are reported in Table 1. The equations relative to the electrolyte-layer/membrane interface were similar. No partition effect was included and the diffusion coefficients of the reduced and oxidized forms were assumed to be equal for all the compounds. In these equations, some values of $\phi^2_{1\mathrm{mo}}$, $\phi^2_{2\mathrm{mo}}$, $Da_{1\mathrm{mo}}$

Table 1. Transient Mass Balance Equations

Reactive Layer

$$\frac{\partial S}{\partial T} = Di^*_S \frac{\partial^2 S}{\partial X^2} - R_1^{ho} \qquad \frac{\partial \mathrm{Red}_1}{\partial T} = Di^*_{\mathrm{Ox}1} \frac{\partial^2 \mathrm{Red}_1}{\partial X^2} \gamma_1 R_1^{ho} - R_2^{ho}$$

$$\frac{\partial \mathrm{Ox}_1}{\partial T} = Di^*_{\mathrm{Ox}1} \frac{\partial^2 \mathrm{Ox}_1}{\partial X^2} - \gamma_2 R_1^{ho} + R_2^{ho} \qquad \frac{\partial \mathrm{Red}_2}{\partial T} = Di^*_{\mathrm{Ox}2} \frac{\partial^2 \mathrm{Red}_2}{\partial X^2} + \gamma_2 R_2^{ho}$$

$$\frac{\partial \mathrm{Ox}_2}{\partial T} = Di^*_{\mathrm{Ox}_2} \frac{\partial^2 \mathrm{Ox}_2}{\partial X^2} - \gamma_2 R_2^{ho}$$

Membrane-Diffusion Layer Interface

$$Di^s_S \left.\frac{\partial S}{\partial X}\right|_{X=(Li+1)^+} = Di^m_S \left.\frac{\partial S}{\partial X}\right|_{X=(Li+1)^-} + R_1^{he}$$

$$Di^s_{\mathrm{Ox}1} \left.\frac{\partial \mathrm{Red}_1}{\partial X}\right|_{X=(\mathrm{Li}+1)^+} = Di^m_{\mathrm{Ox}1} \left.\frac{\partial \mathrm{Red}_1}{\partial X}\right|_{X=(\mathrm{Li}+1)^-} - \gamma_1 R_1^{he} + R_2^{he}$$

$$Di^s_{\mathrm{Ox}1} \left.\frac{\partial \mathrm{Ox}_1}{\partial X}\right|_{X=(\mathrm{Li}+1)^+} = Di^m_{\mathrm{Ox}1} \left.\frac{\partial \mathrm{Ox}_1}{\partial X}\right|_{X=(\mathrm{Li}+1)^-} + \gamma_1 R_1^{he} - R_2^{he}$$

$$Di^s_{\mathrm{Ox}2} \left.\frac{\partial \mathrm{Red}_2}{\partial X}\right|_{X=(\mathrm{Li}+1)^+} = Di^m_{\mathrm{Ox}2} \left.\frac{\partial \mathrm{Red}_2}{\partial X}\right|_{X=(\mathrm{Li}+1)^-} - \gamma_2 R_2^{he}$$

$$Di^s_{\mathrm{Ox}2} \left.\frac{\partial \mathrm{Ox}_2}{\partial X}\right|_{X=(\mathrm{Li}+1)^+} = Di^m_{\mathrm{Ox}2} \left.\frac{\partial \mathrm{Ox}_2}{\partial X}\right|_{X=(\mathrm{Li}+1)^-} + \gamma_2 R_2^{he}$$

Enzymatic Kinetics

Homogeneous	Heterogeneous
$R_1^{ho} = \phi^2_{1mo} \dfrac{1}{1 + \dfrac{K'_S}{S} + \dfrac{K'_{\mathrm{Ox}1}}{\mathrm{Ox}_1}}$	$R_1^{he} = Da_{1mo} \dfrac{1}{1 + \dfrac{K'_S}{S} + \dfrac{K'_{\mathrm{Ox}1}}{\mathrm{Ox}_1}}$
$R_2^{ho} = \phi^2_{2mo} \dfrac{1}{1 + \dfrac{K'_{\mathrm{Red}1}}{\mathrm{Red}_1} + \dfrac{K'_{\mathrm{Ox}2}}{\mathrm{Ox}_2}}$	$R_2^{he} = Da_{2mo} \dfrac{1}{1 + \dfrac{K'_{\mathrm{Red}1}}{\mathrm{Red}_1} + \dfrac{K'_{\mathrm{Ox}2}}{\mathrm{Ox}_2}}$

*The subscript m or s relative to the membrane or the electrolyte layer, respectively.

or Da_{2mo} must be set equal to zero according to the location of the enzymes in the sensor.

At the electrode surface, boundary conditions are imposed by the electrochemical reactions. S, Red_1, and Ox_1 are not electroactive; therefore, their mass flux are nil

$$\left.\frac{\partial S}{\partial X}\right|_{X=0} = 0 \tag{4}$$

$$\left.\frac{\partial \mathrm{Red}_1}{\partial X}\right|_{X=0} = 0 \tag{5}$$

$$\left.\frac{\partial \mathrm{Ox}_1}{\partial X}\right|_{X=0} = 0 \tag{6}$$

The mass flux of the oxidized and reduced forms of the electroactive species are opposite

$$\left.\frac{\partial \mathrm{Ox}_2}{\partial X}\right|_{X=0} = -\left.\frac{\partial \mathrm{Red}_2}{\partial X}\right|_{X=0} \tag{7}$$

The electrochemical reaction is assumed to be fast enough for the concentration of Red_2 to be nil at the electrode

$$\mathrm{Red}_2|_{X=0} = 0 \tag{8}$$

Current density is provided by

$$\Psi = Di^s_{\mathrm{Ox2}} \left.\frac{\partial \mathrm{Red}_2}{\partial X}\right|_{X=0} \tag{9}$$

When the electrolyte layer between the electrode and the membrane is neglected for Type-2, -3, and -4 sensors, the reactive surface is directly applied against the electrode and the expression for the current density becomes

$$\Psi = Di_{\mathrm{Ox2}} \left.\frac{\partial \mathrm{Red}_2}{\partial X}\right|_{X=0} + Da_{2\mathrm{mo}} \frac{1}{1 + \dfrac{K'_{\mathrm{Red1}}}{\mathrm{Red}_1|_{X=0}} + \dfrac{K'_{\mathrm{Ox2}}}{\mathrm{Ox}_2|_{X=0}}} \tag{10}$$

At the diffusion-layer/solution interface, the concentrations are assumed to be constant during the assay

$$X = Li + 1 + Lo \tag{11}$$

$$\mathrm{Red}_1 = 0 \tag{12}$$

$$\mathrm{Ox}_1 = \mathrm{Ox}_1^b \tag{13}$$

$$S = S^b \tag{14}$$

$$\mathrm{Red}_2 = 0 \tag{15}$$

$$\mathrm{Ox}_2 = 1 \tag{16}$$

The equations of Table 1 associated with the boundary conditions (Eq. 4–Eq. 10) were solved numerically by a finite volume method. These methods are based on an integral form of the partial derivative equations. The computational domain is divided into elementary volumes within which the integration is performed between a west (w) and an east (e) frontier. For example, the substrate mass-balance equation is

$$\frac{\partial}{\partial T}\int_W^e S\,dX = Di^*_S \int_w^e \frac{\partial^2 S}{\partial X^2}\,dX - \phi^2_{1mo}\int_w^e \frac{1}{1 + \dfrac{K'_S}{S} + \dfrac{K'_{\mathrm{Ox1}}}{\mathrm{Ox}_1}}\,dX \tag{17}$$

The integrals were calculated using a piecewise linear profile. The nonlinear kinetic terms were linearized by a first-order Taylor's expansion. The application of this method to such a geometrical system has already been described (Bacha et al., 1993). An important advantage, with respect to classic finite difference methods, is that the space discretization scheme can be chosen without any constraints. It is therefore possible to freely reduce or enlarge the space steps, in any part of the integration domain, without modifying the equations. A smaller mesh can be specified in the vicinity of all the reactive interfaces where steep gradients occur. A typical space discretization is shown in Figure 1. A fine or very fine mesh was chosen at the electrode surface and on both sides of the reactive surfaces, respectively.

Experimental Studies

General

The whole enzymatic system corresponded to a *D*-lactate bienzymatic amperometric sensor. The two successive reactions were

$$D\text{-lactate} + \mathrm{NAD}^+ \xrightarrow{E_1} \mathrm{Pyruvate} + \mathrm{NADH} + \mathrm{H}^+$$

$$\mathrm{NADH} + 2\mathrm{Fe(CN)}_6^{3-} \xrightarrow{E_2} \mathrm{NAD}^+ + 2\mathrm{Fe(CN)}_6^{4-} + \mathrm{H}^+$$

where E_1 was *D*-lactate dehydrogenase and E_2 diaphorase. The detection was based on the oxidation of hexacyanoferrate (II)

$$\mathrm{Fe(CN)}_6^{4-} \rightarrow \mathrm{Fe(CN)}_6^{3-} + e^-$$

on a platinum electrode maintained at a potential of 0.35 V/SCE (Saturated Calomel Electrode) by a Taccussel PRT potentiostat. The monoenzymatic system, which used NADH as substrate, involved only the second enzymatic reaction and the electrochemical detection of $Fe(CN)_6^{4-}$. Diaphorase (E.C. 1.8.1.4.) from *Clostridium kluyveri*, *D*-lactate dehydrogenase (E.C. 1.1.1.28) from *Leuconostoc mesenteroides*, *D*-lactate, NAD^+ and hexacyanoferrate were purchased from Sigma. The monoenzymatic experiments were performed with 0.1-M pH 7.5 phosphate buffer or 0.1-M pH 9.1 carbonate buffer for free or immobilized enzymes, respectively. The bienzymatic experiments were performed in 0.05-M, pH 9.0 AMPSO buffer. The sensor body consisted of a 2-mm^2 platinum bar sealed in a Plexiglas cylinder. The membrane was mechanically held against the top of the sensor by a silicone O-ring. A cellophane membrane of 40-μm dry thickness was used for

free enzyme sensors. The immobilized enzyme sensors were built with an Immunodyne preactivated membrane (Pall Industries) of 150-μm dry thickness. The preactivated surface of this membrane allowed diaphorase and *D*-lactate dehydrogenase to be covalently linked according to the protocol already described (Montagné et al., 1993). The auxiliary electrode was a platinum wire wound around the body of the sensor.

Determination of the physicochemical parameters

The diffusion coefficient of hexacyanoferrate in solution was known from the literature (Weast, 1987). The diffusion coefficient of NADH in solution was measured by a platinum rotating disc electrode according to Levich's equation (Bard and Faulkner, 1980). The diffusion coefficients of NADH and hexacyanoferrate in the membranes were measured with a membrane-covered rotating electrode, according to the method described by Gough and Leypoldt (1979). The activities of the free (r_{max}^{ho}) and the immobilized (r_{max}^{he}) enzymes were measured spectrophotometrically. The enzyme activity units are defined as the amount of enzyme able to catalyze, at 25°C, the oxidation of 1 μmol of NADH per min for the diaphorase, and of 1 μmol of *D*-lactate per min for the *D*-lactate dehydrogenase. All the measurement protocols have have been described elsewhere (Montagné et al., 1993). The Michaelis constants of the diaphorase relative to hexacyanoferrate and NADH were determined experimentally by an usual Lineweaver-Burk procedure (Dixon and Webb, 1979). Values of 0.4 mM and 0.5 mM were obtained, respectively. They were used to fit the experimental results concerning the monoenzymatic sensor. All the Michaelis constants were set to 0.5 mM in the theoretical discussion devoted to bienzymatic reactors. All the values used in the simulation are reported in Tables 2 and 3.

Results and Discussion

Model validation

A free-enzyme device (Type 6) was used with the monoenzymatic system involving NADH as the species to be assayed. Initial conditions were chosen, which gave the most reproducible experimental results and resulted in specific transient behaviors. The sensor was first stabilized in a solution containing only 0.31-mM NADH (Red_1). At the outset, it was plunged into another solution containing NADH and hexacyanoferrate(III) (Ox_2). The initial conditions were

$$0 < X < Li + 1 + Lo \qquad Red_1 = Red_1^b \qquad (18)$$

$$X < Li + 1 \quad \text{(in the device)} \qquad Ox_2 = 0 \qquad (19)$$

$$X > Li + 1 \quad \text{(out of the device)} \qquad Ox_2 = 1 \qquad (20)$$

Figure 3 depicts the experimental and calculated current-time curves obtained with the parameter values reported in Table 2 and for different $Fe(CN)_6^{3-}$ concentrations. As many parameters as possible were determined by independent experiments to ensure significant comparison between the numerical model and experimental data. Except for the minor correction made to the membrane thickness (45 μm instead of 40 μm in dry thickness) which could be related to swelling, only the thickness δ_i of the reactive layer was adjusted numerically by trial and error. It was very shallow (4.5 μm) because the membrane was applied directly against the electrode without any spacer. The thickness of the diffusion layer was also an unknown parameter, but it only had a slight effect on the results because the greater mass-transfer hindrance was located in the membrane: a variation of δ_o from 10 to 100 μm only affected the computed values of the current by less than 4%. The value of 60 μm agreed reasonably well with the low experimental stirring. Thus, the calculated curves fitted experimental data well, with physically significant values of the adjusted parameters.

The transient part of the curve was very sensitive to the kinetic parameters. The Michaelis constant were varied from 0.1 mM to 1 mM, which represents a typical range (Barman, 1985). The value of the peak intensity, computed with NADH 0.31 mM and $Fe(CH)_6^{3-}$ 3.0 mM, varied from +61% to −25%, and from +35% to −16%, for K_{NADH} and $K_{Fe(CH)_6^{3-}}$, respectively, whereas the steady-state value remained practically constant. This confirms that the steady-state behavior of the sensor is strictly mass-transfer-limited, as must be the case for a reliable device.

Table 2. Parameters Used in Simulation of the Free Monoenzymatic Sensor

	Diffusion Coefficients, D ($m^2 \cdot s^{-1}$)	
	NADH	$Fe(CN)_6^{3-}$
Solution	$D^s_{Red1} = 4.5\times10^{-10}$ ($Di^s_{Red1} = 9.5$)	$D^s_{Ox2} = 11.8\times10^{-10}$ ($Di^s_{Ox2} = 25.2$)
Cellophane Membrane	$D^m_{Red1} = 0.24\times10^{-10}$ ($Di^m_{Red1} = 0.5$)	$D^m_{Ox2} = 0.47\times10^{-10}$ ($Di^m_{Ox2} = 1$)
	Kinetics, r^{ho}_{max} ($mol \cdot m^{-3} \cdot s^{-1}$)	
Diaphorase (E_2)	$r^{ho}_{max} = 1.35$ (ϕ^2_{2mo}: variable)	
$K_{Red1} = 0.5$	$K_{Ox2} = 0.4$ (K' variable)	
Stoichiometric Coefficient	$\gamma_2 = 2$	
	Geometry, δ (μm)	
Electrolyte Layer	Membrane	Diffusion Layer
$\delta_i = 4.5$ ($Li = 0.1$)	$\delta_m = 45$	$\delta_d = 60$ ($Lo = 1.3$)
	Concentrations [ ] ($mol \cdot m^{-3}$)	
NADH		$Fe(CN)_6^{3-}$
$[Red_1]^b = 0.31$ (Red_1^b: variable)		$[Ox_2]^b$ variable

*Dimensionless parameters are in parentheses.

Table 3. Parameters Used to Simulate Immobilized-Enzyme Sensors

Diffusion Coefficients, D ($m^2 \cdot s^{-1}$)			
	Lactate	NADH	$Fe(CN)_6^{3-}$
In the solution	$D_S^s = 15.0 \times 10^{-10}$ ($Di_S^s = 8.1$)	$D_{Red1}^s = 4.5 \times 10^{-10}$ ($Di_{Red1}^s = 2.4$)	$D_{Ox2}^s = 11.8 \times 10^{-10}$ ($Di_{Ox2}^s = 6.4$)
In the Pall membrane	$D_S^m = 1.77 \times 10^{-10}$ ($Di_S^m = 1$)	$D_{Red1}^m = 0.65 \times 10^{-10}$ ($Di_{Red1}^m = 0.4$)	$D_{Ox2}^m = 1.85 \times 10^{-10}$ ($Di_{Ox2}^m = 1$)
Kinetics, r_{max}^{ho} ($mol \cdot m^{-2} \cdot s^{-1}$)			
Monoenzymatic sensor	*D*-lactatedehydrogenase (E_1) no		Diaphorase (E_2) $r_{max}^{he} = 7.5 \times 10^{-4}$ $Da_{2mo} = 21.6$
Bienzymatic sensors	$r_{max}^{he} = 2.1 \times 10^{-4}$ ($Da_{1mo} = 18.2$)		$r_{max}^{he} = 7.5 \times 10^{-4}$ ($Da_{2mo} = 64.9$)
All the K: 0.5 $mol \cdot m^{-3}$	($K' = 0.025$)		
Stoichiometric coefficients	$\gamma_1 = 1$		$\gamma_2 = 2$
Geometry, δ (μm)			
Monoenzymatic sensor	Electrolyte layer $\delta_i = 0$ ($Li = 0$)	Membrane $\delta_m = 160$	Diffusion layer $\delta_d = 20$ ($Li = 0.12$)
Bienzymatic sensors	$\delta_i = 10$ ($Li = 0.06$)	$\delta_m = 160$	$\delta_d = 15$ ($Li = 0.09$)
Concentrations [ ] ($mol \cdot m^{-3}$)			
Monoenzymatic sensor	NADH $[Red_1]^b$ variable		$Fe(CN)_6^{3-}$ $[Ox_2]^b = 30$
Bienzymatic sensors	*D*-lactate $[S]^b$ 0.1 ($S^b = 0.01$)	NAD^+ $[Ox_1]^b = 10$ ($Ox_1^b = 10$)	$Fe(CN)_6^{3-}$ $[Ox_2]^b = 10$

*Dimension parameters are in parentheses.

This type of peak-shaped current-time curve is very rare in the area of biosensor studies. Most often, the transient current increases continuously until a steady-state plateau is reached. Current peaks have already been noted with a glucose biosensor, but they are induced by variations in bulk concentrations and not by the coupled mass-transfer/kinetic phenomena within the microdevice (Lucisano and Gough, 1988). The evolution of the concentration profiles of NADH (Red_1) and $Fe(CH)_6^{4-}$ (Red_2) in the reactive layer and the membrane ($0 < X < Li + 1$) are plotted in Figure 3 for $Fe(CH)_6^{3-} = 3.0$ mM. The substrate Red_1, which was initially contained in the reactive layer, was consumed very quickly by the enzymatic reaction as soon as Ox_2 penetrated the layer by diffusion through the diffusion layer and the membrane, resulting in the initial rapid production of Red_2 and current increase (curves 1, 2, and 3). Diffusion of substrate through the membrane was then not able to compensate its depletion in the reactive layer. Evolution of the Red_2 concentration profiles clearly explained the current decay (curves 4, 5, and 6). This behavior could have an important practical interest for improving sensor performances, because a peak value would be easier to measure than a steady-state value and it would give a shorter response time.

It was not possible to obtain experimentally a similar transient behavior with enzyme-immobilized microdevices. The preactivated membranes, which were used to link the enzymes, were too thick and hindered mass transfers too much to allow an initial rapid current increase. The device was initially stabilized in solution without the substrate Red_1, which was added at the outset. According to the experimental protocol, the initial conditions were

$$0 \le X < Li + 1 + Lo: \quad Red_1 = 0 \tag{21}$$

$$X = 1: \quad Red_1 = Red_1^b = \frac{[Red_1]^b}{[Ox_2]^b} \tag{22}$$

$$0 \le X \le Li + 1 + Lo: \quad Ox_2 = 1 \tag{23}$$

where Red_1 and Ox_2 were still NADH and $Fe(CH)_6^{3-}$, respectively. The evolution of the experimental steady-state current as a function of NADH concentration is plotted in Figure 4. The solid line represents the calculated results obtained with the physicochemical parameters reported in Table 3. As previously noted, the kinetic parameters and the diffusion coefficients were determined by independent experiments. δ_i was set equal to 0. The dry thickness of 150 μm was slightly modified to 160 μm, but only the thickness of the diffusion layer was really adjusted numerically by trial and error. The value of 20 μm for δ_o corresponded to strong stirring as was the case experimentally. The deviation observed for high NADH concentrations could be explained by enzyme inhibition due to the formed NAD^+, which was not incorporated in the model.

Figure 4 also shows the transient current evolution obtained with two different bienzymatic immobilized enzyme sensors which used *D*-lactate as substrate. Diaphorase (E_2) was always linked to the inner membrane surface, i.e., the side against the electrode. *D*-lactate dehydrogenase (E_1) was linked either to the inner membrane surface (Type 2), or to the outer surface (Type 3). Calculations were made with the same parameter values as previously (Table 3). It was not possible to determine experimentally the diffusion coefficients of *D*-lactate by the same method as for the other diffusion coefficients, because it is not an electroactive species. The diffusion coefficient of *D*-lactate in solution 15.0×10^{-10} $m^2 \cdot s^{-1}$ was derived from a previous fitting obtained with a

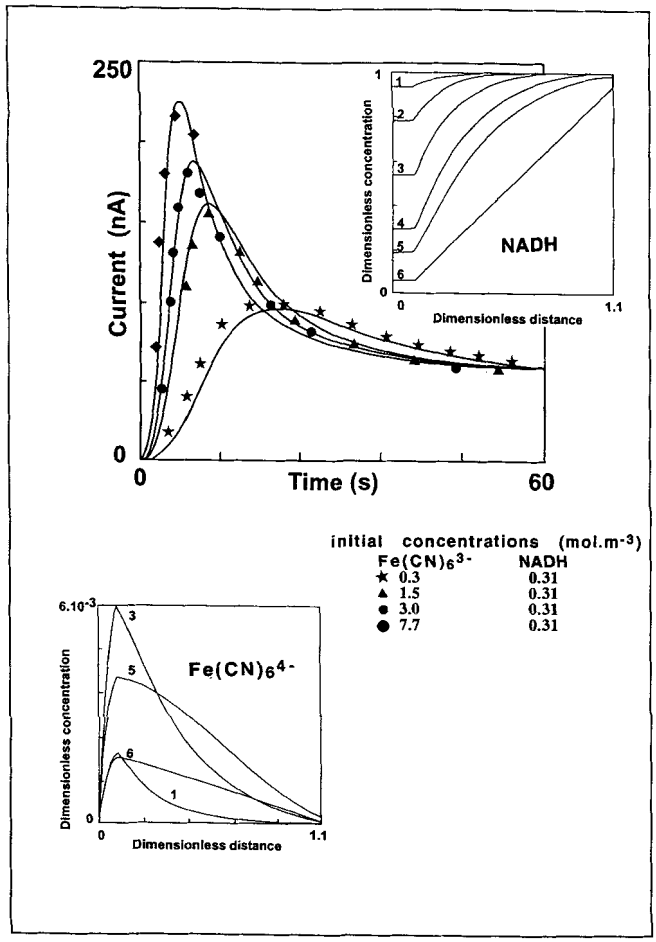

Figure 3. Free-enzyme sensor (Type 6).

Comparison of experimental (points) and theoretical (solid lines) results. The parameter values are reported in Table 2. The concentration profiles of NADH (Red_1) and $Fe(CH)_6^{4-}$ (Ox_2) are plotted for the initial concentration $Fe(CN)_6^{3-}$ = 3.0 mM at times: (1) 3.6 s; (2) 5.4 s; (3) 7.8 s; (4) 11.4 s; (5) 15.0 s; (6) 60 s.

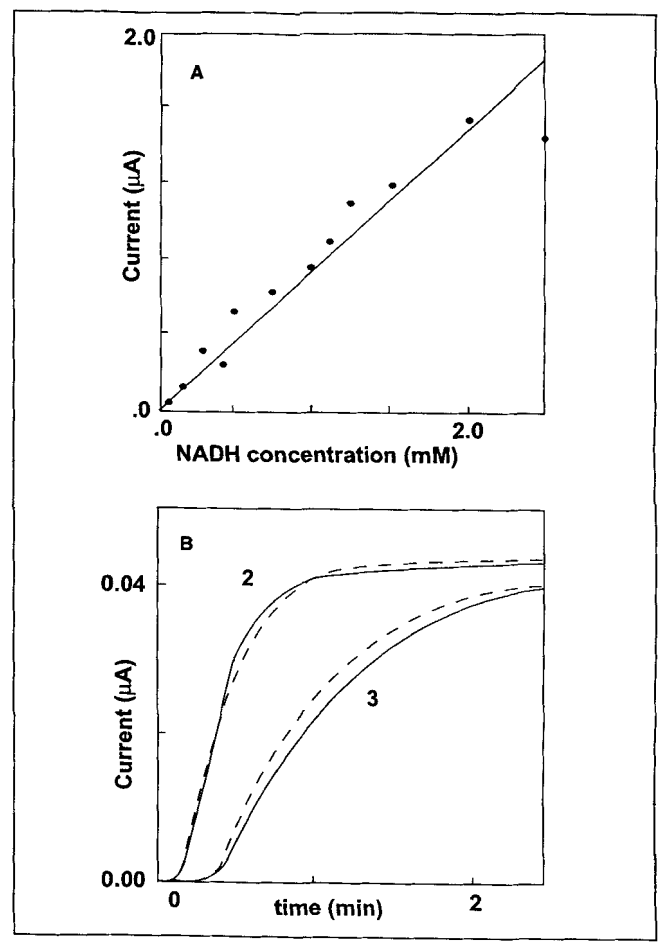

Figure 4. Immobilized-enzyme sensors.

(A) Comparison of experimental (points) and theoretical (line) steady-state response of a monoenzymatic immobilized sensor (Type 1 with diaphorase only); (B) comparison of experimental (dashed lines) and theoretical (solid line) transient response of Type-2 and Type-3 bienzymatic immobilized sensors. The parameters values are reported in Table 3.

free-enzyme device involving the bienzymatic system. The value in the membrane was numerically adjusted by trial and error to 1.77×10^{-10} $m^2\cdot s^{-1}$. δ_i and δ_o were only slightly modified. Correction of δ_i from 0 to 10 μm corresponded to a real experimental difficulty in reproducing this layer from one device to another. Similarly, δ_o was set to 15 μm instead of 20 μm, no doubt due to poor control of the stirring conditions. Actually this parameter only had significant influence on the response of the Type-3 sensor. The model showed that free- and immobilized-enzyme devices, with no enzyme linked to the solution/membrane interface, are more suitable for model validation because they are only very slightly sensitive to stirring conditions. The physical consistency of all the adjusted parameters confirmed that the model satisfactorily fits the experimental transient behavior of these devices.

Model predictions relative to bienzymatic immobilized systems

Transient behavior of microreactors could reveal a great number of different patterns according to the coupled effects of their geometry and different mass-transport conditions. The five types (1 to 5) of previously described bienzymatic sensors with immobilized enzymes were considered and combined with the three mass-transport conditions reported in Table 4

(A) All the species have normal mass-transfer features

(B) Mass transfer of the substrate S is slow

(C) Mass transfers of the substrate S and of the mediator Red_1 are both slow.

Figure 5 compared the performances of the five sensors under the mass-transport conditions of Case A. The Type-2 sensor ensured the fastest and highest current response. All the reactive processes occurred at the electrode surface in this device; there was consequently no loss of species Red_2 by diffusion back to the bulk of the solution as this occurred in the other devices, resulting in a drastic decrease in the response of Type-1 sensor. The discrepancy between Types 1 and 2 demonstrates the great importance of the choice of enzyme location in the device. Moreover, comparison with the current-time responses, which were calculated under the mass-transport conditions of Case B, showed that designing the microdevices must also account for the properties of the

Table 4. Dimensionless Parameters Used to Simulate Various Mass-Transfer Conditions

	Diffusion Coefficients		
Case A	$Di_S^s = 20$ $Di_S^m = 10$	$Di_{Ox1}^s = 20$ $Di_{Ox1}^m = 10$	$Di_{Ox2}^s = 10$ $Di_{Ox2}^m = 1$
Case B	$Di_S^s = 0.5$ $Di_S^m = 0.1$	$Di_{Ox1}^s = 20$ $Di_{Ox1}^m = 10$	$Di_{Ox2}^s = 10$ $Di_{Ox2}^m = 1$
Case C	$Di_S^s = 0.5$ $Di_S^m = 0.1$	$Di_{Ox1}^s = 0.5$ $Di_{Ox1}^m = 0.5$	$Di_{Ox2}^s = 10$ $Di_{Ox2}^m = 1$
	Kinetics		
	$\phi_{1mo}^2 = Da_{1mo} = 0.1$ and $\phi_{2mo}^2 = Da_{2mo} = 10$		
All the K': 0.025 stoichiometric coefficients		$\gamma_1 = 1$	$\gamma_2 = 1$
	Geometry		
Electrolyte layer $Li = 0$	Membrane 1		Diffusion layer $Lo = 1$
	Concentrations		
$S^b = 0.05$	$Ox_1^b = 1$		$Ox_2^b = 1$

physicochemical system to be processed. In this case, the Type-2 sensor was drastically hindered by the slow diffusion of S through the membrane and only gave a low current, whereas Type 3 was the most efficient. Actually, the Type-3 sensor combined two advantages in Case B. On the one hand, the substrate, which had the worst mass-transport properties, reacted on the outer side of the membrane and did not have to diffuse through the membrane. The Red_1 species, with better mass-transport properties, ensured the diffusion to the electrode. On the other hand, the electroactive species Red_2 was only generated on the inner side of the membrane, in direct contact with the electrode surface. There was no diffusion of this electroactive species back to the solution.

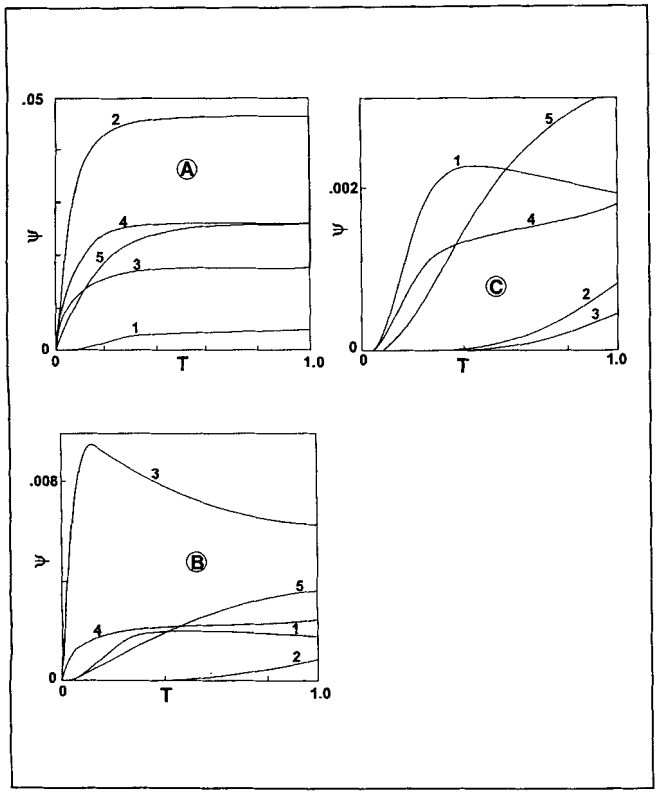

Figure 5. Theoretical current-time responses of immobilized enzyme sensors (Type 1 to 5).

The parameters used for the three Cases A, B and C are reported in Table 4.

Comparison of the behaviors of Type-3 and -4 sensors in Cases A and B also emphasized the difficulty in making qualitative predictions without any theoretical model. Case A indicated that addition of enzyme in order to transform Type 3 into Type 4 improved the response. Case B showed the opposite effect. When enzyme E_2, which catalyzed the transformation of Red_1 into Red_2, was also present on the outer membrane surface, most of the Red_1 generated at this interface was immediately transformed into Red_2 and was lost for detection by diffusion to the bulk of the solution. In this case, multiplying the enzyme linkages on all the reactive sites in the hope of enhancing the reactive process was detrimental to the performances of the device. It is also worth noting the shape of the response curve of the Type-4 sensor in Case B, which showed the superposition of a first fast response similar to that of Type 3, over a second one corresponding to the slow diffusion of substrate S through the membrane.

Comparison of Cases B and C showed that the same features which ensured the high performances of Type 3 in Case B can also become detrimental to it under the mass-transport conditions of Case C. When both S and Red_1 had very low transport rates (Case C), the amplitude of the response of all the sensors decreased considerably, but Type 3 was affected the most. In this case, the main preoccupation must be to ensure that only the species with acceptable mass-transport properties diffused through the membrane. This was achieved by Type 1, which transformed a great part of S into Red_2 as soon as it reached the outer side of the membrane.

In Case C, the Type-1 sensor exhibited a response curve with a maximum as was the case with a few previous responses. Examining the concentration profiles at three times, prior to the current maximum (a), close to it (b) and after it (c), demonstrated that this phenomenon was similar to those encountered with free-enzyme sensors (Figure 6). The enzymatic system rapidly consumed the substrate S initially present in the diffusion layer that resulted in a great Red_2 production and a gradient increase at the electrode surface. Then, the diffusion of the species was not able to compensate the substrate depletion and the high reaction rates could no longer be maintained. The Red_2 concentration gradient decreased at the electrode surface.

For analytical purposes, mastering the conditions required for obtaining a response curve with a transient maximum could offer a relevant opportunity to improve biosensor performance. Unfortunately, it was very difficult to recover this shape of the response curve experimentally with immobilized-enzyme devices. This behavior depends on the amount of substrate initially present in the diffusive layer compared to the consumption rate. The curves were calculated with quite a large diffusive layer thickness ($Lo = 1$, resulted in $\delta_d = \delta_m$), which was difficult to achieve experimentally with immobilized-enzyme devices because of the excessive thickness of commercially available membranes. Because of the enhanced performances this transient behavior could offer, a systematic study is now in progress to define precisely the

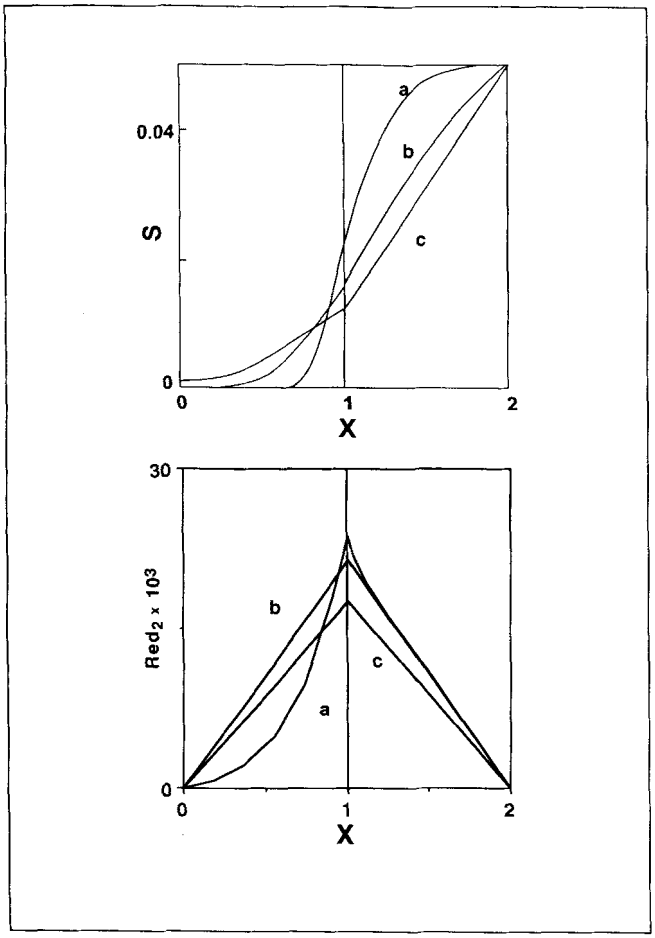

Figure 6. Evolution of the concentration profiles of S and Red_2 for Type 1 sensor under mass-transfer conditions of Case C.

(a) T = 0.1; (b) T = 0.245; (3) T = 1.

conditions necessary for obtaining a reproducible maximum, as was the case with monoenzymatic free enzyme sensors.

Conclusion

A first insight into transient behavior of electroenzymatic microreactors was proposed on the basis of the available simple technology of enzymatic biosensors. The different geometrical and physicochemical features, kinetic properties, or operating conditions multiply the number of cases to be studied. Comparison between experimental and theoretical results were made with different sensor types under different conditions. Unfortunately, the simple technology used here did not ensure strict reproducible values of the geometrical parameters and some corrections were necessary from one microdevice to the other. The examples covered here clearly show that it is very difficult to predict qualitatively the behavior of these microdevices by simple rules of thumb. Two sensor types which at first glance could appear very similar can lead to quite different responses. The best way to design and optimize a microreactor appears to model all the suitable arrangements, once most of the parameter values have been estimated. In this way, the model proposed here can be a useful tool, particularly due to the great versatility provided by the numerical integration method.

The greatest difference between these biosensors and future possible microreactors is undoubtedly the substrate feeding mode. Diffusion from the bulk through a diffusion layer should be replaced by feeding with microfluidic devices. On the other hand, electrochemical monitoring was found to be a promising means for microreactor analysis because of the possibility of continuously monitoring the mass flux of the electroactive species. Moreover, because of the restricted dimensions and the very high surface-volume ratio of these reactors, the electrochemical conditions could not only affect the strict vicinity of the electrode, but also monitor the whole reactive volume. This might, for instance, allow homogeneous reactions to be easily driven far from thermodynamic equilibrium.

Acknowledgment

This work was supported in part by a financial grant from the Ministère de la Recherche et de la Technologie within the framework of the program "Instrumentation et Capteurs." The authors are grateful to Pr. H. Durliat and Pr. M. Comtat for their help.

Notation

$Da_{i,\mathrm{mo}}$ = modified Damköhler number, $Da_{i,\mathrm{mo}} = (r^{he}_{i,\max}\,\delta_m)/D^m_{\mathrm{Ox2}}[\mathrm{Ox}_2]^b)$
D = diffusivity, $\mathrm{m}^2\cdot\mathrm{s}^{-1}$
Di = dimensionless diffusivity, $Di = D/D^m_S$
F = Faraday's constant, $\mathrm{C}\cdot\mathrm{mol}^{-1}$
i = current density, $\mathrm{A}\cdot\mathrm{m}^{-2}$
$K'_S, K'_{\mathrm{Ox}}, K'_{\mathrm{Red}}$ = dimensionless Michaelis constants, $K' = K/[\mathrm{Ox}_2]^b$
Li, Lo = dimensionless thickness of the electrolyte layer and the diffusion layer respectively, $Li = \delta_i/\delta_m$, $Lo = \delta_d/\delta_m$
$r^{ho}_{\max}, r^{he}_{\max}$ = homogeneous and heterogeneous activity of the enzymes, $\mathrm{mol}\cdot\mathrm{m}^{-3}\cdot\mathrm{s}^{-1}$ and $\mathrm{mol}\cdot\mathrm{m}^{-2}\cdot\mathrm{s}^{-1}$
R^{ho}, R^{he} = homogeneous and heterogeneous enzymatic rates, $\mathrm{mol}\cdot\mathrm{m}^{-3}\cdot\mathrm{s}^{-1}$ and $\mathrm{mol}\cdot\mathrm{m}^{-2}\cdot\mathrm{s}^{-1}$ (defined in Table 1)
$S, \mathrm{Ox}, \mathrm{Red}$ = dimensionless concentrations of S, Ox, Red, $S = [S]/[\mathrm{Ox}_2]^b$
$[S], [\mathrm{Ox}], [\mathrm{Red}]$ = concentration of S, Ox, Red, $\mathrm{mol}\cdot\mathrm{m}^{-3}$
t = time, s
T = dimensionless time, $T = tD^m_S/\delta^2_m$
x = distance from the electrode, m
X = dimensionless distance from the electrode, $X = x/\delta_m$
z = number of electrons exchanged

Greek letters

γ_1, γ_2 = stoichiometric coefficients
$\delta_i, \delta_m, \delta_d$ = thickness of the electrolyte layer, the membrane, the diffusion layer respectively, m
$\phi_{i,mo}$ = modified Thiele modulus, $\phi^2_{\mathrm{mo}} = (r^{ho}_{i,\max}\,\delta^2_m)/(D^m_{\mathrm{Ox2}}[\mathrm{Ox}_2]^b)$
ψ = dimensionless current density, $\psi = (i\,\delta_m)/(zFD^m_S[\mathrm{Ox}_2]^b)$

Subscript and superscripts

$1, 2$ = relative to the first and second enzymatic catalysis
b = in the bulk of the solution
s, m = relative to the solution and the membrane respectively
he, ho = heterogeneous, homogeneous

Literature Cited

Bacha, S., A. Bergel, and M. Comtat, "Modeling of Amperometric Biosensors by a Finite-Volume Method," *J. Electroanal. Chem.*, **359**, 21 (1993).

Bard, A. J., and L. R. Faulkner, *Electrochemical, Methods, Fundamentals and Applications*, Wiley, New York, p. 407 (1980).
Barman, T. E., *Enzyme Handbook*, 2nd ed., Springer-Verlag, New York (1985).
Bauer, R., D. K. Friday, and D. J. Kirwan, "Mass Transfer and Kinetic Effects in an Electrode-Driven Homogeneous Reaction," *Ind. Eng. Chem. Fundam.*, **20**, 141 (1981).
Buerk, D. G., *Biosensors. Theory and Applications*, Technomic Publishing, Lancaster (1993).
Devaux, R., A. Bergel, and M. Comtat, "Mass Transfer with Chemical Reaction in Thin-Layer Electrochemical Reactors," *AIChE J.*, **41**, 1944 (1995).
Dixon, M., and E. C. Webb, *Enzymes*, 3rd ed., Longman Group Ltd., London (1979).
Ehrfeld, W., R. Einhaus, D. Münchmeyer, and H. Strathmann, "Microfabrication of Membranes with Extreme Porosity and Uniform Pore Size," *J. Memb. Sci.*, **36**, 67 (1988).
Ehrfeld, W., and G. Wegner, "Microsystem Technology for Chemical and Biological Microreactors," Dechema e.V. Workshop, Mainz, Germany (1995).
Gass, V., B. H. Vanderschoot, S. Jeanneret, and N. F. Derooij, "Integrated Flow-Regulated Silicon Micropump," *Sensors and Actuators A-physical*, **43**, 335 (1994).
Gough, D. A., and J. K. Leypoldt, "Membrane-Covered Rotated Electrode," *Anal. Chem.*, **51**, 439 (1979).
Gough, D. A., and J. K. Leypoldt, "A Novel Rotated Disc Electrode and Time Lag Method for Characterizing Mass Transport in Liquid-Membrane Systems," *AIChE J.*, **26**, 1013 (1980).
Labrune, P., and A. Bergel, "Modelling of an Indirect Electrosynthesis Process—I. Theoretical Study of the Effect of Dismutation of the Mediator," *Chem. Eng. Sci.*, **47**, 1219 (1992).
Laviron, E., and L. Roullier, "The Square Scheme with the Electrochemical Reactions at Equilibrium. A Study by Diffusion or Thin Layer Cyclic Voltammetry and by Scanning Potential Coulometry," *J. Electroanal. Chem.*, **186**, 1 (1985).
Lucisano, J. Y., and D. A. Gough, "Transient Response of the Two-Dimensional Glucose Sensor," *Anal. Chem.*, **60**, 1272 (1988).
Montagné, M., H. Durliat, and M. Comtat, "Simultaneous Use of Dehydrogenases and Hexacyanoferrate(III) ion in Electrochemical Biosensors for L-lactate, D-lactate, and L-glutamate ions," *Anal. Chim. Acta*, **278**, 25 (1993).
Patankar, S. V., *Numerical Heat Transfer and Fluid Flow*, W. J. Minkowycz and E. M. Sparrow, eds., Hemisphere Publishing Corp., New York (1980).
Plichon, V., and E. Laviron, "Theoretical Study of a Two-Step Reversible Electrochemical Reaction Associated with Irreversible Chemical Reactions in Thin Layer Linear Potential Sweep Voltammetry," *J. Electroanal. Chem.*, **71**, 143 (1976).
Scheller, F., and F. Schubert, *Biosensors*, Elsevier, Amsterdam (1992).
Shih, T. M., *Numerical Heat Transfer*, W. J. Minkowycz and E. M. Sparrow, eds., Hemisphere Publishing Corp., New York (1984).
Tse, P. H. S., J. K. Leypoldt, and D. A. Gough, "Determination of the Intrinsic Kinetic Constants of Immobilized Glucose Oxidase and Catalase," *Biotechnol. Bioengin.*, **29**, 696 (1987).
Van de Pol, F. C. M., H. T. G. Van Lintel, M. Elwenspoek, and J. H. J. Fluitman, "A Thermopneumatic Micropump Based on Micro-engineering Techniques," *Sensors and Actuators*, **A21–A23**, 198 (1990).
Walker, I., B. H. Vanderschoot, S. Jeanneret, P. Arquint, N. F. Derooij, V. Gass, B. Beckler, B. Lorenzi, and A. Gogoli, "Development of a Miniature Bioreactor for Continuous Culture in a Space Laboratory," *J. Biotechnol.*, **38**, 21 (1994).
Weast, R. C., *Handbook of Chemistry and Physics*, 68th ed., CRC Press Inc., Boca Raton, FL, p. F47 (1987).
Weise, L., G. Valentin, and A. Stork, "Selectivity Analysis in Electrochemical Reactors: II. Engineering Models of a Batch Reactor with a Complex Reaction Sequence," *J. Appl. Electrochem.*, **16**, 851 (1986).

Manuscript received Nov. 29, 1995, and revision received Mar. 18, 1996.